Natural Resources Canada | Ressources naturelles Canada

GEOMATICS CANADA
OPEN FILE 39

Relationship between leaf area index and Landsat Operational Land Imager equivalent reduced simple ratio vegetation index for the Athabasca oil sands region, northern Alberta

R.A. Fernandes, M. Maloley, and F. Canisius

2018

Canada

GEOMATICS CANADA
OPEN FILE 39

Relationship between leaf area index and Landsat Operational Land Imager equivalent reduced simple ratio vegetation index for the Athabasca oil sands region, northern Alberta

R.A. Fernandes, M. Maloley, and F. Canisius

2018

Permanent link: https://doi.org/10.4095/308333

This publication is available for free download through GEOSCAN (http://geoscan.nrcan.gc.ca/).

Recommended citation
Fernandes, R.A., Maloley, M. and Canisius, F., 2018. Relationship between leaf area index and Landsat Operational Land Imager equivalent reduced simple ratio vegetation index for the Athabasca oil sands region, northern Alberta; Geomatics Canada, Open File 39, 34 p. https://doi.org/10.4095/308333

Publications in this series have not been edited; they are released as submitted by the author.

Abstract

This document describes the production of a regression relationship between leaf area index and the reduced simple ration vegetation index (RSR) for Landsat Operational Land Imager spectral bands over the Athabasca Oil Sands region of Alberta. from satellite imagery using standard Canada Centre for Remote Sensing algorithms. 245 Elementary Sampling Units (ESUs) were specified based on a stratification of both land cover and spectral reflectance in the vicinity of Fort McKay, Alberta, Canada. ESU LAI was estimated using in-situ digital hemispherical photographs acquired during the 2012 and 2013 growing seasons. The estimation used the CCRS Line Transect protocol followed by processing using CANEYEV6.3 software. Empirical corrections for shoot clumping are documented. In-situ Lai ranged from 0.09 to 6.08. A SPOT 5 satellite image was acquired within two weeks of each of the 2012 and 2013 field campaigns, orthorectified to within 10m (1 standard deviation) and radiometrically normalized to invariant targets in a surface reflectance Landsat OLI image acquired within 1 week of the 2013 SPOT image. The RSR was derived from both normalized SPOT5 images and sampled over each ESU. A Thiel-Sen linear regression was applied to generate a relationship to predict LAI given RSR across all sampled land cover conditions with a root mean square error of 0.49.

1. Introduction

The Athabasca Oil Sands (AOS) region of Alberta has the 3rd largest proven reserves of oil in the world. A comprehensive monitoring effort led by the Governments of Canada and Alberta is underway to track the status of the ecosystem. Numerical models are being used to assess environmental impacts on air, water and ecosystems. Many of these models require time series of gridded land surface parameters including Leaf Area Index (LAI). LAI is defined as half the total foliage area per unit horizontal ground area (Chen and Black, 1992; Fernandes et al., 2014).

Empirical relationships between spectral vegetation indices based on satellite imagery and LAI have been used previously for producing LAI time series maps over Canada (Chen et al., 2002; Fernandes et al. 2003). The reduced simple ratio (RSR) vegetation index (VI) derived from Landsat Thematic Mapper data has been shown to be almost linearly related to LAI over Boreal forests with low sensitivity to land cover or understory variation (Brown et al. 2000; Stenberg et al.2004). In this study a relationship between LAI and RSR for Landsat Operational Land Imager (OLI) equivalent spectral bands suitable for the AOS region is developed. This relationship can be used to produce LAI maps over the study region from surface reflectance derived from Landsat OLI measurements.

2. Study Area

The study area of ~600km^2 is located north of Fort McMurray, Alberta, in the AOS (Fig. 1). The study area falls within the Boreal Plains ecozone, where cool summers and long cold winters characterize the sub-humid, mid-boreal ecoclimate type with mean annual temperature of 0.5 and mean annual precipitation ranging from 350 to 500 mm. Dominant vegetation types are medium to closed canopy stands of aspen balsam poplar, white spruce, black spruce and balsam fir. Wetlands consist of fens and bogs with tamarack and black spruce. Organic soil is dominant covering 50% of the region. Disturbances are predominantly due to forest fires and oil and gas exploration (Pickell et al., 2015). Disturbed areas transition from exposed to grass cover, followed by shrubs and broadleaf forest cover and eventually mixed conifer stands.

Figure 1. Location of Athabasca Oil Sands region.

3. Methodology

A LAI versus RSR regression equation was calibrated using in-situ LAI estimates and the RSR vegetation index from remotely sensed spectral data. Land cover maps were used for stratification of LAI sampling and for uncertainty statistics.

3.1. LAI Sampling

A total of 245 ESUs were sampled across the study area (Figure 2). The sampling was divided over two summers, with 165 ESUs in 2012 and 80 in 2013. The number of ESUs was constrained by resources for in-situ measurement.

A circa 2010 30m resolution land cover map of the region from Landsat Thematic Mapper was acquired from the Alberta Biodiversity Monitoring Institute (Government of Alberta, 2013) to aid in stratification of in-situ sampling sites. The overall thematic accuracy of the map, as estimated by an extensive validation dataset, is 75% with 11 classes. The classes were converted to six Generalized Land Cover

(GLC) classes used for in-situ sample stratification: conifer dominant forest, broadleaf dominant forest, grassland, exposed, wetland, and regeneration. A minimum mapping unit of 2ha was adopted.

A 10m resolution land cover map of the region produced from the July 7, 2012 SPOT5 imagery was produced by Canada Centre for Remote Sensing (Latifovic and Pouliot, 2014) to provide a definitive GLC map co-incident with validated LAI products. Accuracy assessment is ongoing but assessments of maps in the same biome produced with the same methods but at 30m resolution found overall accuracy was 90.3% with a Kappa of 0.898 for 28 land cover classes (Latifovic and Olthof, 2004). The map was used to verify the stratification of measurements by GLC and to summarize uncertainty statistics.

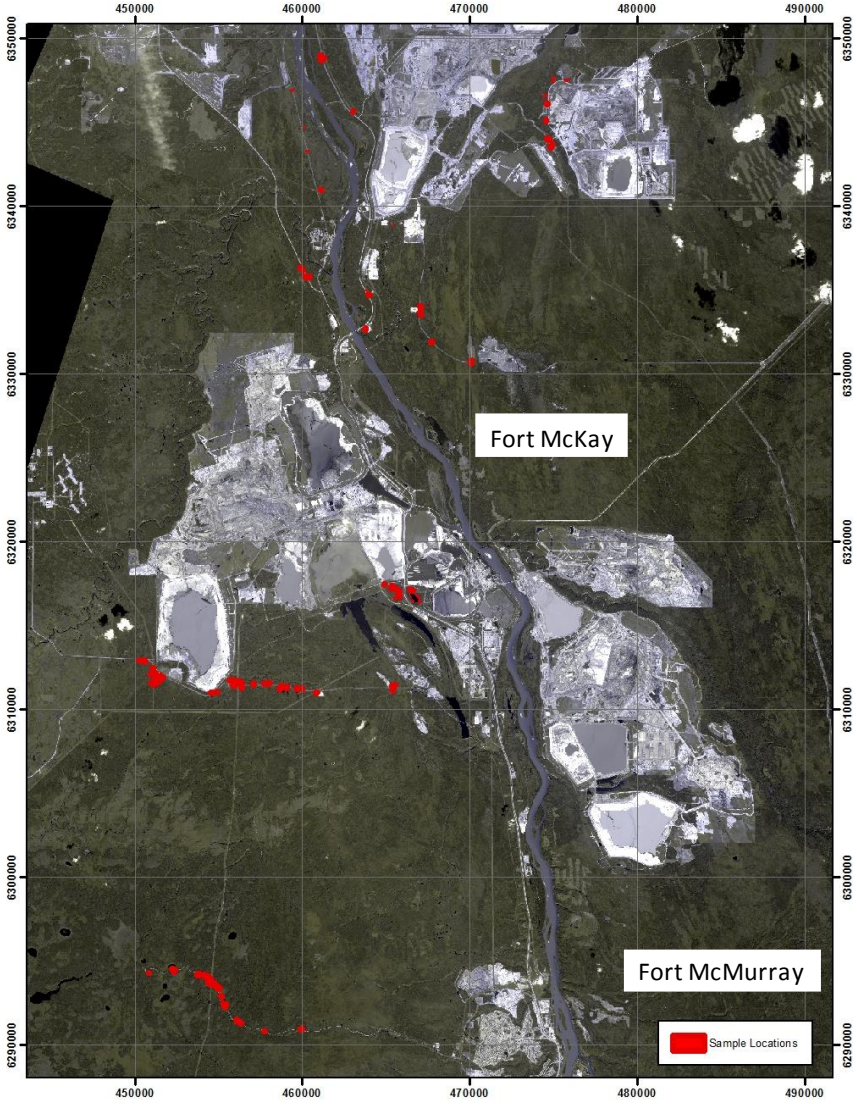

Figure 2. SPOT 5 image, August 10, 2013 together with LAI Elementary Sample Units.

3.2. In-Situ Measurements

In-situ LAI was estimated using digital hemispherical photographs (DHP) following the CCRS protocol described here. The CCRS Protocol estimates the LAI over a region corresponding to a 3x3 no minal pixel region, or Elementary Sampling Unit (ESU), of the multispectral imagery from which RSR values are derived. The protocol covers DHP Acquisition and DHP Analysis.

3.2.1. DHP Acquisition

The goal of DHP acquisition is to produce a single match-up between an in-situ LAI estimate and a satellite VI measurement within an ESU. The CEOS best practice guide for global LAI product validation (Fernandes et al. 2014) identifies a number of within ESU sampling schemes. Here, the CCRS Transect approach was used here to simplify transit within each ESU. This approach uses four 50m long linear transects grouped into two pairs (Figure 3) with a between (within) pair separation of 25m (10m). Hereafter, each pair of transects separated by 10m are termed a 'plot' and the two plots in an ESU are termed an 'ESU'. Previous studies using the CCRS Transect approach estimated the LAI for each plot and then compared the ESU average LAI to VIs estimated form the average surface reflectance of all pixels within a 1ha square centred on the centroid of all transects (e.g. Canisius et al., 2012). Considering the potential for increased spatial variation in LAI near disturbances, spatial match-ups were performed by explicitly considering the overlap of each in-situ DHP measurement footprint and each satellite measurement footprint assuming nadir view angle.

The spatial footprint of each DHP depends on the camera orientation, the angular extent of the DHP field of view used for PAI estimation (FOV) and the distance between the furthest canopy element and the camera lens (d). For simplicity the camera was mounted on a monopod held horizontally by the operator pointing either upward or downwards as indicated by a three axis bubble level. Nadir corresponds to the principal axis of the lens in the pointing direction. The FOV was restricted during subsequent digital processing to exclude the both azimuthal quadrant containing the operator and zenith angles >60°. The zenith angle constraint was based on four requirements: i) the DHP analysis algorithm required measurements at 57.5° ii) minimization of regions without canopy gaps larger than a single DHP pixel iii) minimization of uncertainty of the spatial coverage of the FOV due to camera levelling errors and iv) minimization of the FOV area falling outside the nominal ESU when surveying tall canopies.

The spatial footprint of a single FOV corresponds to a cone, with one quadrant missing, with base radius ~1.7 d. For upward (downward) pointing, d corresponds to the canopy (lens) elevation minus the lens (ground) elevation. For upward (downward) pointing, the monopod usage resulted in a lens height ranging from near ground level (~10cm) to shoulder height (~1.5m). Four considerations were used to specify lens height:

- For canopies where most gaps are small and shadowed (e.g. dense grasses) DHP resolution was maximized by adjusting lens height so as to minimize d.
- For other canopies lens height was adjusted to maximize d to increase the spatial footprint.
- For ESUs with both upward and downward pointing DHP measurements the value of lens height was held constant avoid missing or double counting foliage.
- Irrespective of other requirements, lens height was constrained to ensure a minimum canopy-lens separation within the FOV of 20 leaf widths at nadir and 5 otherwise to satisfy the assumptions of the DHP analysis algorithm (Liang and Xiang, 1986).

These considerations led to the following cases for camera position:

- Canopies <=1m: pointing down at lens height of 20 leaf widths
- Canopies >1m with no understory: pointing up at lens height of 10cm
- Canopies >1m with understory: pointing up and pointing down at each sample location at lens height 50cm.

Where required the camera was shifted horizontally by up to 50cm along the transect to ensure a minimum separation between canopy and lens.

The number of DHP samples in an ESU, n, was determined by balancing available resources against the need to reduce PAI estimation uncertainty. There are three sources of uncertainty: i) due to sampling rather than exhaustive measurement of the angular distribution of gaps over the FOV of pixels overlapping in-situ measurements, ii) measurement error of LAI and iii) errors in modelling the overlap area of in-situ and satellite measurements. The 95%ile upped bound on the spatially random component of the sampling uncertainty due to the first two sources of uncertainty can be expressed relative to the actual LAI as (Licor, 2002):

$$\delta \approx \frac{s_{\widehat{LAI}}}{\widehat{LAI}} \frac{4}{\sqrt{n}} \quad (1)$$

where $\widehat{LAI}$ is the estimated PAI and $s_{\widehat{LAI}}$ is the standard error of the estimated PAI for in-situ measurements in the ESU. Analysis of previous DHP data in Canadian Boreal forests (Abuelgeisum et al. 2006) indicates that within this biomes typical values of δ are $\sim 0.5/\sqrt{n}$ for closed canopies and $\sim 1/\sqrt{n}$ for open canopies. As such $n = 24$ ($n = 45$) is used for closed (open) canopies corresponding to a sampling uncertainty of ~10% (15%). Multiple DHP images also reduces some of the random error due to spatial mismatch of in-situ LAI measurements and satellite pixels although this cannot be estimated a priori since it is sensitive to the relative alignment of the pixel sampling grid (for example Figure 3 shows a potential worst case). The systematic error component within an ESU was approximated as the difference in either LAI or VI between plots and applied, together with estimates of uncertainty in shoot clumping corrections, when calibrating the transfer function (see Section 3.4).

DHP samples were regularly spaced along each transect both to minimize any tendency for operators to preferentially sample vegetation condition and to maximize the potential sampling error in the absence of knowledge of the PIFOV of satellite pixels within the ESU. The start and end point of each transect was recorded using a Garmin Rino 600 GPS instrument with (1 accuracy of 3.6 m; Garmin Inc., 2011). In addition, each camera system was connected to a Nikon GP1 GPS device (1 accuracy <10m Nikon Inc. 2009). In some cases, GP1 measurements were not available for all DHPs on a transect. Missing sample locations were manually interpolated between the two nearest locations on the same transect.

Figure 3 shows an example of a 100m square ESU with a 10m tall canopy typical of forested GLC within the study region. The 24 DHP FOV's (dashed circles) provide sufficient overlap to cover the ESU except for a 10m border strip. The strip is intentional to minimize sampling outside the ESU. With taller canopies DHP FOVs may fall outside the ESU. These FOVs are masked during post-processing if they extend to an area with subjectively different GLC and LAI than the ESU (e.g. a road). The red grid superimposed over the ESU corresponds to a hypothetical 10m resolution satellite image with a worst case misalignment. Ideally, satellite measurements over the sampling area should be averaged by weighting by the overlapping extent of their PIFOVs and DHP FOVs. This is non-trivial considering geolocation uncertainty. As a simplification, reflectance measurements of all pixels falling a specified distance from any DHP location were averaged. The distance was defined as the radius of the

FOV rounded up to the nearest 10m. In the case of Figure 3, this leads to the averaging of measurements within satellite pixels corresponding to shaded red squares.

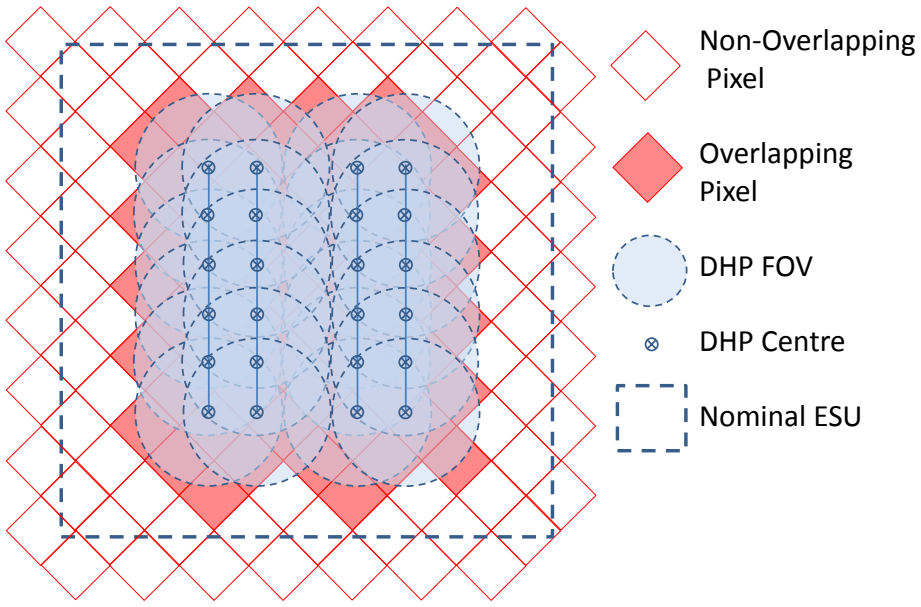

Figure 3. Within ESU sampling for CCRS Transect design with 10m pixels indicated in red. The DHP FOV corresponds to a 10m tall canopy and does not specifically identify masked portions during to CANEYE processing.

DHPs were acquired using different operators for each plot in an ESU. For each plot, a NIKON D7000 Digital Single Lens Reflex (SLR) camera with a AF DX Fisheye-Nikkor 10.5mm f/2.8G ED Lens (Nikon USA, 2014) with a +/-75° horizontal and +/-50° vertical FOV. Cameras were operated in full resolution (4928 horizontal pixels by 3264 vertical pixels) 14bit RAW mode without flash. A number of previous studies suggest DHPs be acquired using a shutter speed two stops slower than that recommended by the camera metering system when in automatic mode (Zhang et al., 2006; Ryu et al., 2010). This recommendation aims to i) ensure that sky regions saturate to improve the accuracy in gap fraction estimation when using a single threshold per channel and ii) to increase the signal to noise ratio of foliage. This recommendation was not followed because i) CANEYEV6.3 DHP analysis software employs an interactive cluster labelling system rather than a single threshold and ii) the cited studies were based on the Nikon CoolPix 4500 that has a dynamic range of ~7.2EV and recorded each colour channel with 8 bits while the D7000 has a significantly larger dynamic range of ~10.5EV and uses 14bits per channel.

Cameras were operated in Programmed Auto mode to allow the D7000 firmware to set the aperture and shutter speed. If the aperture fell below f5.0 the shutter speed was decreased by up to two stops to

enhance the depth of field. Manual focus was used with the focal distance set as the distance from the lens to the further canopy element along nadir so as to minimize the blurring of foliage elements (see Appendix I). The first overstory and understory DHP in each transect was visually examined to verify and if need be the focus was adjusted.

3.2.2. DHP Analysis

DHPs were analyzed to estimate ESU LAI through three steps: pre-processing of imagery, estimation of plan area index (PAI, corresponding to half the total plant area per unit horizontal ground area), correction of PAI for non-foliage area to estimate LAI.

Pre-Processing of DHPs

DHPs in a plot were separated into either 'up' or 'down' orientations and analyzed separately. DHPs were imported into the Nikon VienwNX2 software (Nikon Inc., http://imaging.nikon.com/ lineup /software/viewnx2/) where the following steps were applied:

- digital correction for chromatic and axial aberration;
- enhancement of region saturated with high ('highlights') or low ('shadows') intensity values;
- D-lighting enhancement to perform local histogram equalization, starting with 50% enhancement with (increased) decreased enhancement if shadows (edges) were visibly blurred (noisy);
- subsampling by a factor of 2 in row and column directions to satisfy computer memory limitations when using CANEYEV6.3;
- exporting in highest quality JPEG format.

Figure 4 provides an example of an input RAW DHP and resulting DHP processed using ViewNX2.

Figure 4. Typical RAW Nikon D7000 DHP image (left) and sub-sampled enhanced JPEG image (right) using ViewNX2.

PAI Estimation

DHPs for a plot were imported into CANEYE 6.3. The steps listed below were applied to estimate PAI.

- The following areas were visually identified for masking: the operator, trunks subtending greater than ~1/16th of the perimeter, foliage elements subtending greater than ~1/16th of the azimuthal or zenithal dimensions and solar blooming through foliage.
- Except for solar blooming, wedge shaped masks extending from the perimeter to the DHP centre were drawn so as to cover areas to be masked. Wedges were used to avoid biased sampling of zenith angles that could impact clumping calculations.
- Solar blooming around foliage was masked by a convex hull.
- Masks of plant elements were doubled in azimuthal width to avoid biasing the remaining unmasked regions due to the removal of plant area from the analysis.
- DHPs were visually assessed for colour balance and if need be reprocessed in ViewNX2 to adjust their colour balance or deleted from processing.
- Interactive cluster labelling of unmasked areas was performed until, on average over the plot, at least 85% of the images were labelled as 'foliage' or 'gap'.
- PAI was estimated from CANEYEV6.3 using a minimum available azimuthal grid cells of 2.5° and zenithal grid cells of 2.5°. The zenith field of view for analysis was limited to +/-60° of nadir to minimize the impact of camera pointing errors on PAI estimation.

Figure 5 provides an example of intermediate steps during CANEYE6.3 processing. Here only one DHP is processed for illustrative purposes although typically 12 or 24 DHPs were processed.

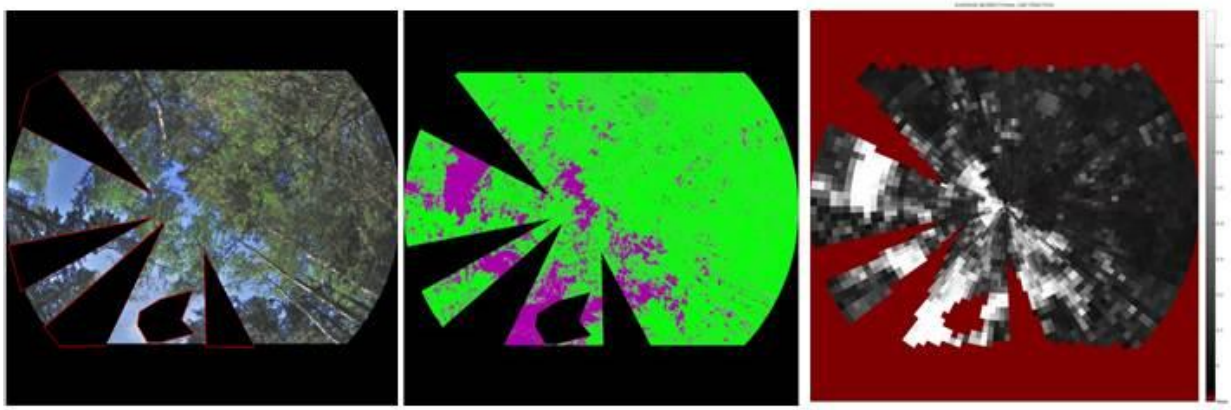

Figure 5. Sample DHP processing for image show in Figure 3 including: a) masked image, b) classified into gap (pink) and plant (green); c) gap fraction image.

The following quality control steps were performed using the output of CANEYE processing:

- If azimuthal grid cells with zero gap fraction occurred the cell size was increased by 0.5° and the plot reprocessed until no saturated cells were reported.
- PAIe computed using only gap fraction estimates 57° zenith angle was compared to the PAIe from the CANEYEV6.3 solution. Plots where PAIe differed by the greater of either 20% or 1 unit of PAIe were reprocessed.
- The measured and modelled gap fraction for a plot was compared. If, for zenith angles between 10° and 60°, the difference between measured and modelled gap fraction exceeded the standard deviation of the measured gap fraction the plot was reprocessed.
- For forested ESUs, overstory plots were reprocessed once when their PAIe differed by more than two standard deviations of their average PAIe. A similar quality control was not implemented for understory plots since the area sampled by an understory plot offered no overlap between transects.
- The plot clumping index, defined as the ratio of PAIe to PAI was computed. The plot was reprocessed if the clumping index fell below 0.4 or above 1.1.

Conversion of PAI to LAI

Conversion from PAI to LAI requires specification of non-foliage to total area ratio, α, and the needle to shoot area ratio, γ_e, that are expected to vary with species, growth stage and site conditions (Chen et al., 2006). DHP analysis can be used to estimate α for broadleaf stands but most areas of the AOS had some evergreen vegetation. Following Kucharik et al. (1998) we only account for the contribution of non-foliage area caused by the portion of tree trunks located below crowns when computing α. The fraction of each DHP between 55° and 60° zenith angle free of trunks was manually estimated. The locations assessed were defined as the centre of a fixed rectangular 9x9 pixel window spanning 57.5° view zenith angle and placed in the eight cardinal directions between within each DHP. In the event the centre of a window was masked it was shifted location to the first unmasked pixel clockwise in azimuth. The gap faction in the window considering only trunks, P_T, was visually estimated from the unmasked pixels in the window. The average gap fraction considering only trunks at 57.5° was taken as the average of these measurements over all DHPs in an ESU. The effective trunk area index (TAIe) at 57.5° was then computed as:

$$TAI_e(57.5°) = -2lnP_T(57.5°)/\cos(57.5°) \qquad (2)$$

LAI was then estimated aa

$$LAI = PAI[1 - TAI_e(57.5°)/PAI_e(57.5°)] \quad (3)$$

corresponding to the assumption that α=$TAIe$(57.5°)/$PAIe$(57.5°). This estimate assumes that the clumping of foliage and woody area is similar at 57.5degrees as has been supported by ray tracing studies over realistic boreal forest canopies (Leblanc, 2014) and has been used by Nilsson et al. (2004) previously over Boreal forests.

Chen and Cihlar (1995) used basal area to weight local measurements of γ_e for species in a plot. Basal area measurements were not conducted. A visual estimate of the relative effective foliage area of needle leaf and broadleaf foliage within DHPs in a plot was performed by randomly sampling 5 foliage pixels spanning a range of zenith angles in each DHP. For ESUs with more than one needle leaf species, a random sample of 10 dominant or co-dominant trees was used to estimate the relative weighing of each species' value given in Table 1.

Table 1. Needle-to-shoot area ratio values used to relate PAI to LAI based on average of growing season measurements

Common Name	Needle-to-shoot area ratio	Reference
Black Spruce	1.42 (1.36-1.50)	Chen et al. 1997
White Spruce	1.27	Hall et al. 2004
Jack Pine >15yrs	1.42 (1.30-1.50)	Chen et al. 1997
Jack Pine <=15yrs	1.40 (1.27-1.52)	Chen et al. 1997
All broadleaf species	1	Chen et al. 1997

3.3. RSR Estimation

RSR was estimated using SPOT 5 HR imagery cross-calibrated to Landsat OLI equivalent surface reflectance. SPOTH5 HR imagery was required due to the lack of Landsat OLI imagery within +/-2 weeks of field measurements.

Satellite Data

SPOT5 HR Level L3A imagery, provided by Iunctus Geomatics, was acquired on July 7th 2012, August 1rst 2013 and August 10th 2013 (Table 2). Level 3A processing corresponds to (http://www.geo-airbusds.com/en/166-spotview):

- Radiometric correction of distortions due to differences in sensitivity of the elementary detectors of the viewing instrument. Intended for users who wish to do their own geometric image processing.
- Geometric correction of systematic effects and internal instrument distortions.
- Map projection based on ground control points and a DEM based on Reference3D data to eliminate distortions due to relief
- Geolocation accuracy of better than 10m (1σ).

A Landsat 8 OLI image from August 8, 2013 (Table 2) was also acquired for the purpose of radiometric normalization of the SPOT imagery.

Satellite Data Processing

The OLI image was atmospherically corrected using the PCI Geomatica implementation of ATCOR3 (Richter and Schlapfer, 2014) with a continental atmosphere model, water vapour taken from NCEP reanalysis products (xx) and aerosol optical depth at 550nm specified using average optical depth over the scene taken from the clear-sky MODIS TERRA optical depth product (MOD04_l2, Levy et al., 2013) closest in time to the OLI overpass. Normalization corresponded to a linear cross-calibration of corresponding spectral bands for red, near infrared (NIR) and shortwave infrared (SWIR) wavelengths (Table 2) of each SPOT top of atmosphere radiance image to a surface reflectance image A 25m digital elevation model (CTI-NRCAN) was used in the correction for terrain effects.

To perform normalization each SPOT image was resampled to the OLI projection. Both the resampled SPOT image and OLI reflectance image were aggregated to 90m resolution using a rectangular moving window average. Five hundred points were randomly sampled in each image in areas that were considered to be relatively invariant over time (GLC corresponding to conifer forests, impervious areas, centres of lakes, and high density broadleaf forests). Linear regressions between the 2012 and 2013 SPOT5 DN and 2013 Landsat 8 OLI reflectance for near infrared (NIR), red, and short-wave infrared (SWIR) bands based on 500 random points within the study area can be seen for in Figures 6 and 7. Despite the year difference between the Landsat and 2012 SPOT imagery, the linear regressions were deemed acceptable with $r2 > 0.90$ for all 3 bands. Saturation of SPOT DNs were noticed but these values are typically on non-vegetated (e.g. impervious) GLC pixels and not likely to be considered in the LAI analysis.

The derived normalization relationships were applied to the original SPOT5 DN bands to produce SPOT5 OLI equivalent reflectance bands. The Reduced Simple Ratio (RSR) was derived from these bands:

$$RSR = \frac{\rho_{NIR}}{\rho_{RED}}\left(\frac{\rho_{SWIR,max}-\rho_{SWIR}}{\rho_{SWIR,max}-\rho_{SWIR,min}}\right) \quad (4)$$

where ρ_{NIR}, ρ_{RED}, and ρ_{SWIR} are the reflectance in near infrared, red, and short-wave infrared bands, respectively and $\rho_{SWIR,min}$ and $\rho_{SWIR,max}$ are the minimum and maximum SWIR reflectance found in vegetated areas of the image .

Table 2. Satellite Data

Sensor	Date	Product ID	Bands
SPOT5 HR	07-07-2012	553723312070718353 82J	10m multispectral
SPOT5 HR	07-07-2012	55372341207071835462J	10m multispectral
SPOT5 HR	01-08-2013	55372341308011820031J	10m multispectral
SPOT5 HR	10-08-2013	55372321308101846132J	10m multispectral
Landsat OLI	08-08-2013	LC80420202013220LGN00	30m multispectral

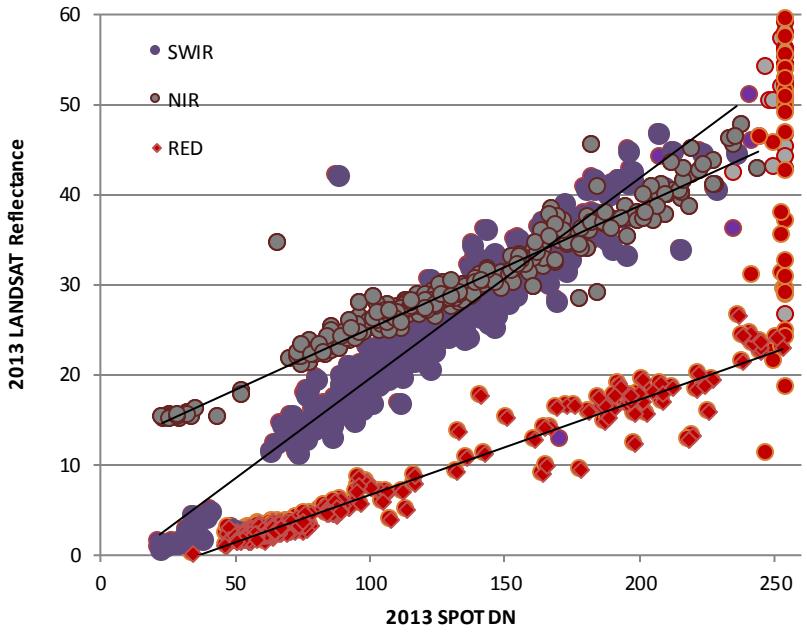

Figure 6. Landsat 8 surface reflectance (August 8th, 2013) and SPOT5 DN (August 1rst 2013 and August 10th 2013).

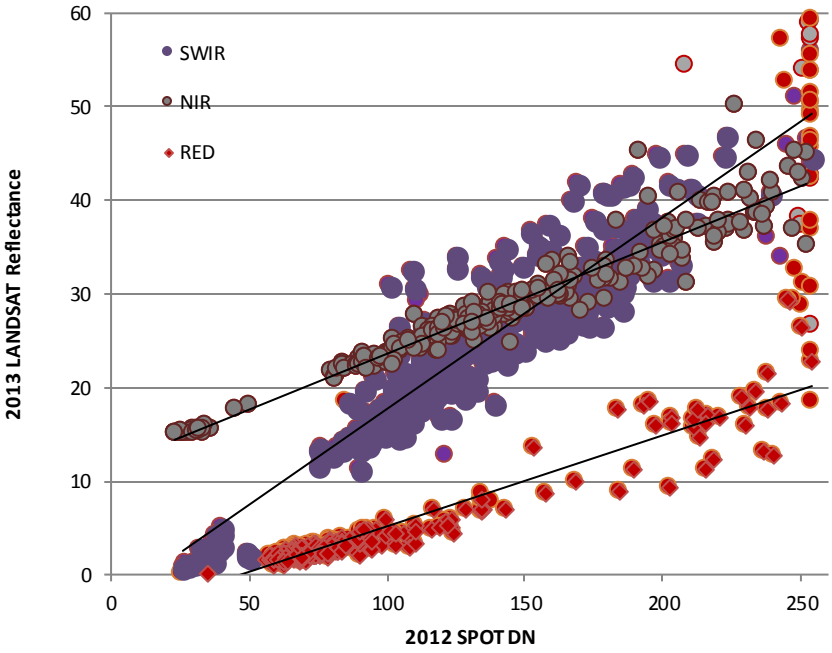

Figure 7. Landsat 8 surface reflectance (August 8th, 2013) and SPOT5 DN (July 7th 2012).

3.4. Regression Calibration

Thiel-Sen regression was used to calibrate a linear predictor of LAI given RSR (Fernandes and Leblanc, 2005). Thiel-Sen regression provides a consistent estimator of this relationship assuming that conditional residuals are independent and identically distributed and that an upper bound on measurement error of LAI and RSR are known.

The measurement of LAI and RSR has both additive and multiplicative errors. The transfer function was calibrated using a range of power transformations until conditional residuals were found to show no obvious trend with LAI based on a visual assessment of a scatter plot of residuals.

An upper bound estimate of LAI measurement error of 1.2 units corresponding to 20% for LAI 6 (close to the maximum LAI) was adopted based on previous validation of CANEYE based LAI estimates (Demarez et al., 2008). An upper bound estimate of RSR measurement error of 20% of the range of RSR was used based on the cross-calibration uncertainty between SPOT5 HR and OLI images.

4. Results

Table 3 summarizes the range of LAI and OLI equivalent RSR over the calibration data set corresponding to the plots listed in Annex 1. Table 4summarizes quartiles in-situ LAI as a function of GLC. LAI ranges from 0.09 (a disturbed site) to 6.08 (a broadleaf forest). As expected, grass and disturbed GLC had the lowest LAI amongst GLC classes for each quartile. Disturbed LAI was higher than grass LAI for higher quartiles as these disturbed sites correspond to regenerating forests. Broadleaf and conifer LAI was similar for quartiles 2 to 4 but broadleaf was lower for the first quartile as this also included shrubs and conifer was slightly lower (<5%) for the highest quartile. The similarity for forested LAI reflects the fact that most stands were actually mixed forests.

The relatively high minimum LAI for conifer indicate a potential for underestimate of non-foliage area in conifer stands. However, the LAI-RSR scatter plot shown in Figure 8 does not show a bias for low LAI conifers suggesting that either the RSR is also responding to non-foliage area or that the underestimate is not large. Figure 3 also suggests are slight bias to higher RSR (~0.5 units) for data acquired in 2013 versus 2012. The bias may be due to the later growing season date for the 2013 SPOT5 image compared to the 2012 image. If so the bias may reflect actual conditions. The scatter in LAI-RSR data increases with

increasing LAI and RSR indicating that multiplicative errors are likely present and supporting the application of power transformations prior to fitting regression curves.

Figure 8 shows scatter plots of power transformed LAI and RSR together with Thiel-Sen regression linear regression for different exponents applied to RSR and LAI. Based on visual examination, an exponent of 0.67 for RSR and LAI was deemed adequate to render residuals approximately independent and identically distributed. and to support a linear relationship.

Table 3. Summary of calibration dataset.

Cover Class	#plots	Min LAI	Max LAI	Min RSR	Max RSR
Broadleaf	109	0.16	6.08	0.90	12.82
Conifer	71	1.86	5.45	3.26	11.30
Disturbed	10	0.09	4.24	0.61	6.58
Grass/Exposed	28	0.26	2.90	0.60	5.11
Wetland	27	1.39	4.69	1.71	11.11
All	245	0.16	6.08	0.60	5.11

Table 4. LAI quartile mean values as a function of GLC.

	LAI Quartile				
GLC	1st	2nd	3rd	4th	All
Broadleaf	1.71	3.35	4.15	5.14	3.57
Conifer	2.94	3.67	4.12	4.72	3.88
Disturbed	0.40	1.37	2.44	3.40	1.94
Grass/Exposed	0.49	1.04	1.71	2.46	1.36
Wetland	2.22	3.23	3.87	4.36	3.45
All	1.41	3.10	3.98	4.86	3.23

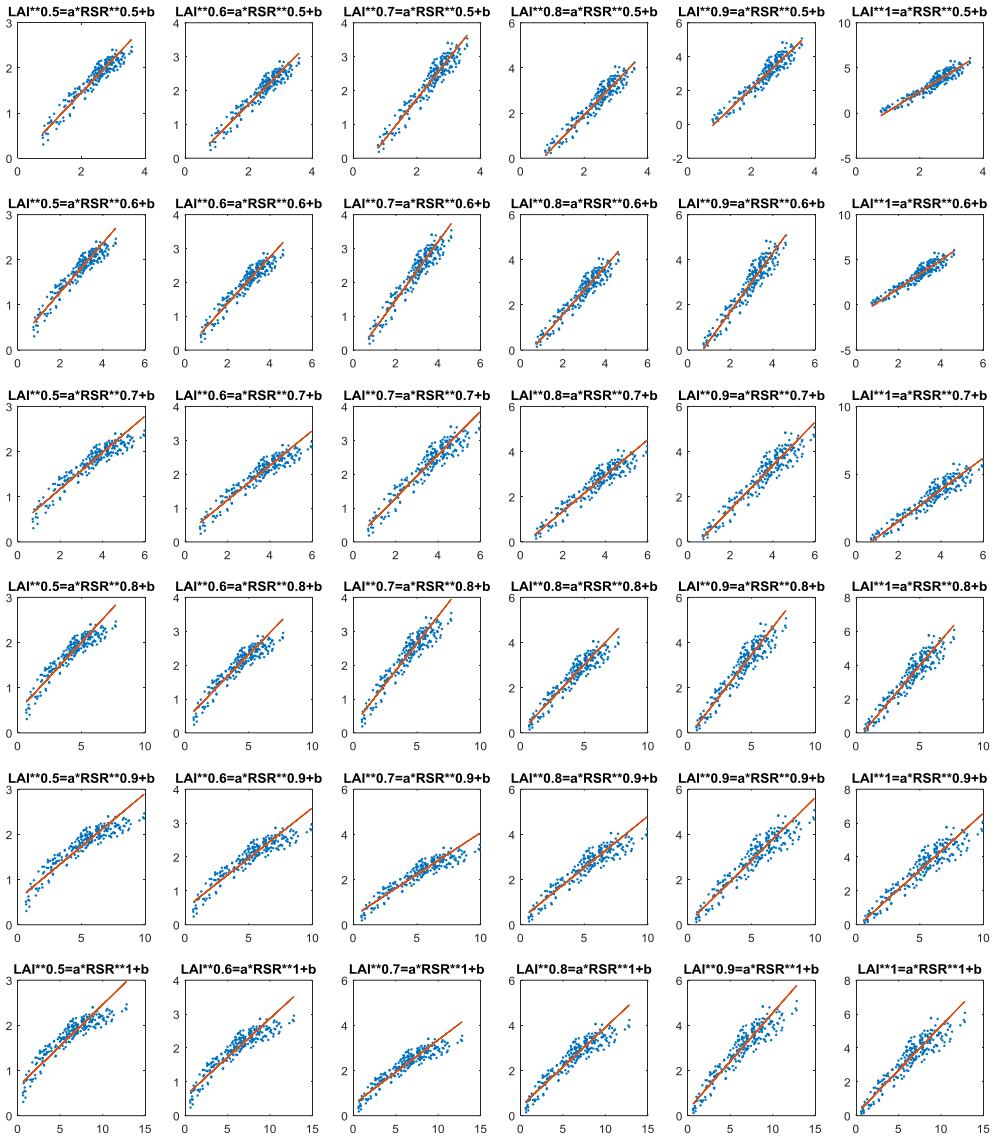

Figure 8. Scatter plots of power transformed LAI versus power transformed RSR for different combinations of exponents ranging from 0.5 to 1.0. Thiel-Sen linear fits are included.

The final regression relationship to predict LAI from OLI RSR for natural vegetated areas of the Athabasca Oil Sands region is (see Figure 9):

$$LAI = (0.65RSR^{0.7} - 0.208)^{1/0.7} \quad (5)$$

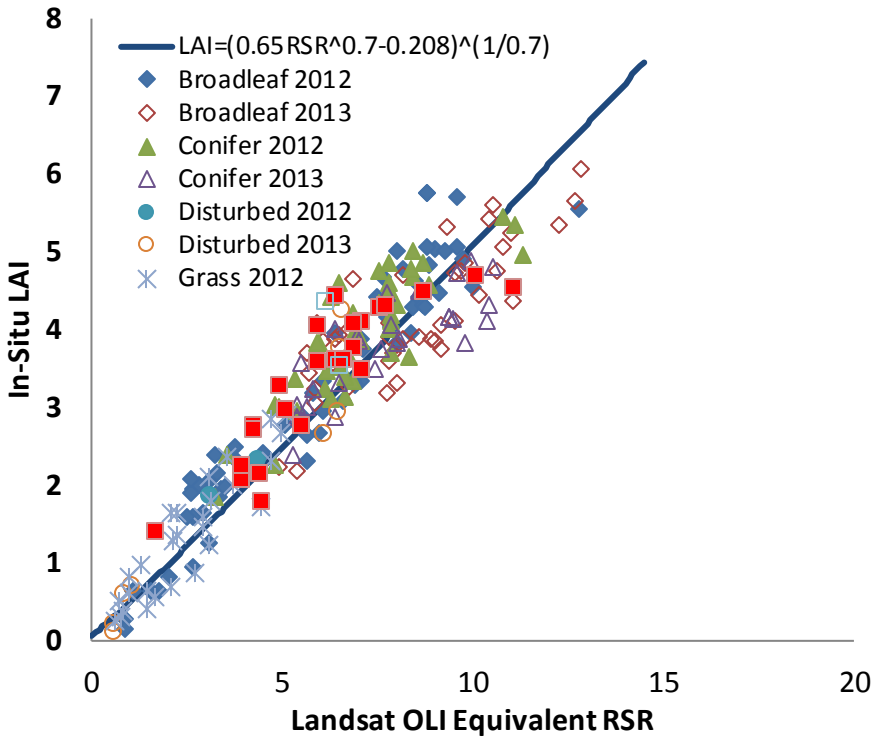

Figure 9. In-situ LAI versus Landsat OLI Equivalent RSR derived from SPOT 5 imagery over Alberta Oil Sands together with linear regression predictor of LAI given RSR.

Table 5 summarizes root mean square error and relative root mean square error as a function of LAI and GLC. RMSE ranges from 0.15 for the lowest quartile disturbed sites, that correspond to essentially barren land, to 0.69 for the highest quartile wetlands, that correspond to treed peatlands. The high RMSE over treed wetlands is expected since the RSR employs a shortwave infrared correction that assumes understory moisture is proportional to understory LAI (Brown et al., 2000) while, in peatlands understory moisture is typically close to saturation or even standing water. LAI product specifications are typically in terms of a maximum RMSE or percentage error (Fernandes et al., 2014). Here the relative error reached 48% for the first quartile of grassland but this reflects the low LAI for this quartile and the fact that the calibration dataset was dominated by forested sites. Even so the worst case error does not exceed 16% or 0.69 LAI units indicating that Equation 8 is suitable if used to produce LAI maps that are aggregated over multiple cover classes or not used for applications requiring high relative accuracy. The analysis was also repeated using the Median Absolute Error with similar results (Table 6) although in some cases the GLC class with worst case errors differed.

Table 5. Root Mean Square Error (RMSE) of LAI Prediction as a function of GLC and LAI quartile. RMSE relative to quartile mean LAI expressed in % given in brackets.

	LAI Quartile				
GLC	1st	2nd	3rd	4th	All
Broadleaf	0.40 (28)	0.49 (14)	0.59 (14)	0.60 (11)	0.52 (14)
Conifer	0.31 (10)	0.52 (14)	0.61 (14)	0.56 (11)	0.51 (13)
Disturbed	0.15 (37)	0.14 (10)	0.45 (18)	0.57 (16)	0.38 (19)
Grass/Exposed	0.24 (48)	0.34 (32)	0.36 (21)	0.27 (11)	0.32 (23)
Wetland	0.38 (17)	0.31 (9)	0.37 (9)	0.69 (15)	0.50 (14)
All	0.35 (24)	0.39 (12)	0.56 (14)	0.63 (13)	0.49 (14)

Table 6. Median absolute error (MAE) of LAI Prediction as a function of GLC and LAI quartile. MAE relative to quartile mean LAI expressed in % given in brackets.

	LAI Quartile				
GLC	1st	2nd	3rd	4th	All
Broadleaf	0.35 (20)	0.43 (12)	0.43 (10)	0.44 (8)	0.41 (9)
Conifer	0.27 (9)	0.42 (11)	0.33(7)	0.38 (8)	0.32 (8)
Disturbed	0.16 (39)	0.15 (11)	0.36 (14)	0.62 (18)	0.18 (17)
Grass/Exposed	0.15 (29)	0.30 (28)	0.14 (8)	0.27 (8)	0.24 (24)
Wetland	0.34 (15)	0.29 (8)	0.25 (6)	0.37 (6)	0.32 (9)
All	0.27 (19)	0.32 (10)	0.43 (10)	0.44 (9)	0.34 (10)

5. Conclusions

A stratified random sampling of the landscape in the Alberta Oil Sands region was used to relate the Landsat OLI equivalent reduced simple ratio vegetation index to leaf area index. PAI was estimated using in-situ digital hemispherical photographs processed using CANEYV6.3. Image based estimates of non-foliage area, corresponding to trunk area and empirical corrections for shoot clumping were applied to convert CANEYEV6.3 PAI estimates to LAI. LANDSAT8 OLI equivalent RSR was estimated from two SPOT5 images cross-calibrated to an OLI image. While there is potential for substantial (up to 20% or 1.2 unit) error in in-situ LAI the errors should be random to a large extent between cover classes and to a lesser extent within cover classes (biases due to clumping may be cover class dependent). A systematic difference of ~0.5 RSR units between years may need further investigation as it could be due to growing season differences or due to calibration target changes.

A single linear relationship between LAI and RSR seems to apply across cover classes with an overall RMSE of 0.49 (14% relative to the mean LAI). This vastly simplifies LAI estimation in the region since cover class data is not required and also increases the precision of the LAI-RSR regression. Further work should verify the relationship with additional satellite and in-situ measurements.

6. References

Abuelgeisum, A., Fernandes, R.A., and Leblanc, S.G., 2006. Evaluation of national and global LAI products derived from optical remote sensing instruments over Canada, IEEE Trans. Geosci. Rem. Sens., 44, 1872-1884.

Brown, L. J., J. M. Chen, and S. G. Leblanc, 2000. Short wave infrared correction to the simple ratio: an image and model analysis. Remote Sensing of Environment, 71,16-25.

Canisius, F., Fernandes, R.A., and Chen J.M., 2010. Comparison and evaluation of medium resolution imaging specrometer leaf area index products across a range of land use. Remote Sensing of Environment, 111, 950-960.

Chen, J. M. and Black, T. A.,1992. Defining leaf area index for non-flat leaves. Plant Cell and Environment. 15: 421-429.

Chen, J. M. and J. Cihlar, 1996. Retrieving leaf area index for boreal conifer forests using Landsat TM images. Remote Sensing of Environment, 55, 153-162.

Chen, J. M., G. Pavlic, L. Brown, J. Cihlar, S.G. Leblanc, H. P. White, R. J. Hall, D. Peddle, D.J. King, J. A. Trofymow, E. Swift, J. Van der Sanden, and P. Pellikka, 2002. Validation of Canada-wide leaf area index maps using ground measurements and high and moderate resolution satellite imagery. Remote Sensing of Environment 80,165-184.

Demarez, V., Duthoit, S., Baret, F., Weiss, M. and Dedieu, G., 2008. Estimation of leaf area and clumping indexes of crops with hemispherical photographs. Agricultural and Forest Meteorology. 148, 644-655

Eriksson, H., L. Eklundh, A. Kuusk, and T. Nilson, 2006. Impact of understory vegetation on forest canopy reflectance and remotely sensed LAI estimates, Remote Sensing of Environment, 103, 408–418.

Fernandes, R. A., C. Butson, S. Leblanc, and R. Latifovic, 2003. A Landsat-5 TM and Landsat-7 ETM+ based accuracy assessment of leaf area index products for Canada derived from SPOT4/VGT data, Can.J. Rem. Sens., 29, 241– 258.

Fernandes, R. A., and S.G. Leblanc, 2005. Parametric (modified least squares) and non-parametric (Theil–Sen) linear regressions for predicting biophysical parameters in the presence of measurement errors, Remote Sensing of Environment 95, 303–316.

Fernandes, R.A., Plummer, S.E., and Nightingale, J.,2014. CEOS Global LAI Product Validation Good Practices, DOI 10.5067/doc/ceoswgcv/lpv/lai.002, 82pp.

Garmin Inc., 2011. Rino 6000 Series Owner's Manual, downloaded from http://support.garmin.com/support/manuals/manuals.htm?partNo=010-00928-00&language=en&country=US on September 30, 2015.

Government of Alberta, 2013. Forest health and adaptation in Alberta, Environment and Sustainable Development Alberta, 52pp.

Kucharik, C. J., Norman, J. M. and Gower, S. T.,1998. Measurements of branch area and adjusting leaf area index indirect measurements. Agricultural and Forest Meteorology. 91, 69-88.
Lang, A. and Xiang, Y.,1986. Estimation of leaf area index from transmission of direct sunlight in discontinuous canopies. Agricultural and Forest Meteorology. 19, 187-207.

Latifovic, R., and Pouliot, D., 2014. Monitoring cumulative long-term vegetation changes over Athabasca Oil Sands region, IEEE JSTARS, 99, doi:10.1109/JSTARS.2014.2321058.

Licor, 2010. LAI-2200 Instruction Manual. 984-10633. LI-Cor Inc.

Nikon Inc., 2009. User's Manual - GP-1 GPS Unit, https://support.nikonusa.com/app/answers/detail/a_id/16260/~/users-manual---gp-1-gps-unit accessed on October 25, 2015.

Olthof, I., D. Pouliot, R. Fernandes and R. Latifovic, 2005. Landsat-7 ETM+ radiometric normalization comparison for northern mapping applications, Remote Sensing of Environment, 95, 388-398.

Pickell, P., Andison, D., Coops, N., Gergel, S., and Marshall, P.,2015.The spatial patterns of anthropogenic disturbance in the western Canadian boreal forest following oil and gas development, Canadian Journal of Forest Research, 10.1139/cjfr-2014-0546.

Ryu,Y., Nilson, T., Kobayashi, H., Sonnentag, P., Law, B.E., Baldocchi, D.D., 2010. On the correct estimation of effective leaf area index: Does it reveal information on clumping effects? Agricultural and Forest Meteorology, 150, 463-472.

Stenberg, P., Rautianen, M., Manninen, T., Volpio, P., Smolander, H., 2004. Reduced simple ratio better than NDVI for estimating LAI in Finnish pine and spruce stands, Silva Fennica, 38, pp. 3-14.

Weiss, M. and Baret, F., 2014., CAN-EYE V6.3 Users Manual, EMMAF Laboratory, https://www6.paca.inra.fr/can-eye accessed on October 25, 2015.

Zhang, Y.Q., Chen, J.M., Miller, J.R., 2005. Determining digital hemispherical photograph exposure for leaf area index estimation. Agricultural and Forest Meteorology, 133, 166–181.

Annex I

ESU details included GLC, gelocation information, survey date for in-situ LAI, in-situ LAI and RSR from Landsat OLI Equivalent SPOT5 imagery within 2 weeks of survey date.

Table A1. LAI and RSR over ESUs. Cover class is based on circa 2012 land cover map. Wetland includes treed peatlands. UTM Zone 15.

Site Name	Cover	UTMx	UTMy	Date	LAI	RSR
CCRS104	Broadleaf	475768.63	6347520.56	22-07-2012	2.35	3.75
CCRS104B	Broadleaf	475768.63	6347520.56	22-07-2012	2.50	3.75
CCRS122	Broadleaf	460951.08	6341028.54	22-07-2012	2.42	4.49
CCRS125	Broadleaf	461166.77	6340873.24	22-07-2012	4.29	8.42
CCRS126	Broadleaf	461106.43	6340990.15	22-07-2012	4.41	8.60
CCRS128	Broadleaf	461151.44	6340931.39	22-07-2012	1.64	2.90
BOR27	Broadleaf	461274.48	6348836.54	23-07-2012	1.84	3.35
BOR27B	Broadleaf	461263.42	6348868.75	23-07-2012	2.38	3.25
CCRS138	Broadleaf	474706.21	6343980.99	23-07-2012	2.05	3.08
CCRS138B	Broadleaf	474706.21	6343980.99	23-07-2012	1.27	3.08
CCRS139	Broadleaf	474705.17	6343995.66	23-07-2012	2.16	3.30
CCRS144	Broadleaf	474920.40	6343699.29	23-07-2012	3.08	6.61
CCRS144B	Broadleaf	474920.40	6343699.29	23-07-2012	3.18	5.81
CCRS146	Broadleaf	474799.39	6343527.07	23-07-2012	3.33	6.05
CCRS146B	Broadleaf	474799.39	6343527.07	23-07-2012	2.96	6.05
CCRS147	Broadleaf	474761.91	6343608.73	23-07-2012	1.94	3.41
CCRS150	Broadleaf	461118.40	6348722.48	23-07-2012	3.87	7.08
CCRS150B	Broadleaf	461118.40	6348722.48	23-07-2012	3.35	7.08
CCRS151	Broadleaf	461080.66	6348774.43	23-07-2012	3.96	8.36
CCRS152	Broadleaf	461092.58	6348946.81	23-07-2012	5.75	8.82
CCRS152B	Broadleaf	461092.58	6348946.81	23-07-2012	5.77	8.82
CCRS153	Broadleaf	461026.35	6348924.22	23-07-2012	4.04	7.85

MATC10	Broadleaf	465775.54	6316997.11	23-07-2012	0.29	0.90
MATC10B	Broadleaf	465775.54	6316997.11	23-07-2012	0.16	0.90
BOR7	Broadleaf	457736.16	6290812.87	24-07-2012	3.96	6.36
BOR7B	Broadleaf	457734.56	6290818.29	24-07-2012	3.76	7.12
CCRS204	Broadleaf	450804.76	6294275.19	24-07-2012	5.06	9.58
BOR38	Broadleaf	463799.00	6335034.00	25-07-2012	2.90	5.34
CCRS220	Broadleaf	466375.55	6317284.26	25-07-2012	5.02	8.03
CCRS221	Broadleaf	466420.37	6317273.25	25-07-2012	0.95	2.66
CCRS222	Broadleaf	466397.44	6317227.24	25-07-2012	1.98	3.49
CCRS223	Broadleaf	466329.74	6317105.18	25-07-2012	4.32	8.70
CCRS224	Broadleaf	466375.20	6317218.31	25-07-2012	5.71	9.60
CCRS225	Broadleaf	466375.61	6317015.39	25-07-2012	2.78	5.07
CCRS226	Broadleaf	466358.22	6317114.25	25-07-2012	2.31	5.63
CCRS228	Broadleaf	466443.83	6317044.79	25-07-2012	1.58	2.64
CCRS230	Broadleaf	466452.81	6317054.16	25-07-2012	0.81	2.04
CCRS231	Broadleaf	466667.47	6317041.52	25-07-2012	0.65	1.78
CCRS232	Broadleaf	466499.98	6317075.77	25-07-2012	1.96	2.66
CCRS233	Broadleaf	466510.63	6317116.09	25-07-2012	0.64	1.10
CCRS236	Broadleaf	466551.75	6317040.27	25-07-2012	0.64	1.54
CCRS240	Broadleaf	466688.22	6317097.76	25-07-2012	2.00	2.83
CCRS241	Broadleaf	466863.47	6316768.66	25-07-2012	4.62	8.50
CCRS242	Broadleaf	466790.09	6316812.57	25-07-2012	4.29	8.73
CCRS243	Broadleaf	466981.46	6316418.50	25-07-2012	4.91	9.77
CCRS244	Broadleaf	466927.96	6316699.24	25-07-2012	5.03	9.00
CCRS248	Broadleaf	466968.96	6316304.18	25-07-2012	3.28	6.92
CCRS249	Broadleaf	466549.75	6316519.89	25-07-2012	4.79	8.16
CCRS250	Broadleaf	466599.49	6316450.12	25-07-2012	4.82	8.87
CCRS251	Broadleaf	465381.86	6338869.58	25-07-2012	4.17	7.77
CCRS276	Broadleaf	460066.51	6344685.73	25-07-2012	2.64	5.67

CCRS18 Navus	Broadleaf	457070.00	6311516.00	30-07-2012	4.43	7.51
CCRS19 Navus	Broadleaf	456112.00	6311631.00	30-07-2012	1.59	2.50
CCRS20 Navus	Broadleaf	456306.00	6311584.00	30-07-2012	5.02	9.26
CCRS200 Navus	Broadleaf	454399.00	6293721.00	30-07-2012	4.56	10.00
CCRS201 Navus	Broadleaf	454446.00	6294036.00	30-07-2012	4.48	9.09
CCRS204 Navus	Broadleaf	459925.00	6290922.00	30-07-2012	5.54	12.80
CCRS21 Navus	Broadleaf	456360.00	6311336.00	30-07-2012	1.91	2.59
CCRS22 Navus	Broadleaf	455898.00	6311480.00	30-07-2012	3.35	6.84
CCRS23 Navus	Broadleaf	455949.00	6311657.00	30-07-2012	5.07	8.80
CCRS24 Navus	Broadleaf	455673.00	6311746.00	30-07-2012	4.67	7.62
CCRS26 Navus	Broadleaf	454545.00	6311004.00	30-07-2012	2.91	5.48
CCRS26 Navus2	Broadleaf	454545.00	6311004.00	30-07-2012	2.07	2.59
CCRS32 Navus	Broadleaf	450559.00	6312895.00	30-07-2012	2.68	5.96
CCRS5 Navus	Broadleaf	454234.00	6294051.00	30-07-2012	3.83	8.01
CCRS7 Navus	Broadleaf	454146.00	6294134.00	30-07-2012	4.09	6.85
FMK_14_T1	Broadleaf	460769.00	6311002.00	04-09-2013	3.06	5.87
FMK_14_T2	Broadleaf	460812.00	6311029.00	04-09-2013	3.94	6.50
FMK_17_T1	Broadleaf	465369.00	6311236.00	04-09-2013	3.85	6.08
FMK_17_T2	Broadleaf	465402.00	6311229.00	04-09-2013	4.66	6.86
FMK_5_T1	Broadleaf	459840.00	6311210.00	04-09-2013	3.61	7.81
FMK_5_T2	Broadleaf	459809.00	6311209.00	04-09-2013	3.58	6.32
FMK_6_T1	Broadleaf	459646.00	6311212.00	04-09-2013	3.97	6.63
FMK_6_T2	Broadleaf	459610.00	6311222.00	04-09-2013	3.87	6.40
FMK_7_T1	Broadleaf	459050.00	6311374.00	04-09-2013	2.23	4.90
FMK_7_T2	Broadleaf	459079.00	6311372.00	04-09-2013	2.18	5.41
FMK_8_T1	Broadleaf	459970.00	6311203.00	04-09-2013	4.08	5.92
FMK_8_T2	Broadleaf	459938.00	6311221.00	04-09-2013	3.70	5.64
FMK_0_T1	Broadleaf	459930.00	6336344.00	05-09-2013	3.18	7.75
FMK_0_T2	Broadleaf	459942.00	6336308.00	05-09-2013	3.69	7.93

FMK_1_T1	Broadleaf	459996.00	6336215.00	05-09-2013	3.75	9.15
FMK_1_T2	Broadleaf	460024.00	6336187.00	05-09-2013	3.24	5.84
FMK_19_T1	Broadleaf	454949.00	6293361.00	05-09-2013	4.76	9.69
FMK_19_T2	Broadleaf	454954.00	6293393.00	05-09-2013	5.07	10.81
FMK_20_T1	Broadleaf	455019.00	6293402.00	05-09-2013	5.25	11.03
FMK_20_T2	Broadleaf	455022.00	6293429.00	05-09-2013	5.65	12.69
FMK_21_T1	Broadleaf	460217.00	6335798.00	05-09-2013	4.38	11.03
FMK_21_T2	Broadleaf	460223.00	6335764.00	05-09-2013	4.45	10.17
FMK_22_T1	Broadleaf	460355.00	6335812.00	05-09-2013	3.90	8.57
FMK_22_T2	Broadleaf	460363.00	6335840.00	05-09-2013	3.81	8.01
FMK_23_T1	Broadleaf	463726.00	6332706.00	05-09-2013	4.09	7.78
FMK_23_T2	Broadleaf	463753.00	6332719.00	05-09-2013	3.91	7.81
FMK_24_T1	Broadleaf	463932.00	6334723.00	05-09-2013	3.25	6.78
FMK_24_T2	Broadleaf	463921.00	6334754.00	05-09-2013	3.43	5.72
FMK_25_T1	Broadleaf	456104.00	6291427.00	05-09-2013	4.75	10.64
FMK_25_T2	Broadleaf	456071.00	6291454.00	05-09-2013	5.42	10.43
FMK_30_T1	Broadleaf	467040.00	6333549.00	05-09-2013	3.88	8.17
FMK_30_T2	Broadleaf	467052.00	6333576.00	05-09-2013	3.31	8.03
FMK_31_T1	Broadleaf	467003.00	6333646.00	05-09-2013	4.74	9.55
FMK_31_T2	Broadleaf	467006.00	6333682.00	05-09-2013	4.06	9.18
FMK_32_T1	Broadleaf	467024.00	6334036.00	05-09-2013	3.87	8.92
FMK_32_T2	Broadleaf	467022.00	6334072.00	05-09-2013	4.11	9.55
FMK_42_T2	Broadleaf	455308.00	6292440.00	05-09-2013	5.34	12.28
FMK_43_T1	Broadleaf	455340.00	6292507.00	05-09-2013	6.08	12.82
FMK_43_T2	Broadleaf	455308.00	6292370.00	05-09-2013	5.59	10.54
FMK_44_T1	Broadleaf	455405.00	6292348.00	05-09-2013	3.85	9.04
FMK_44_T2	Broadleaf	455373.00	6292405.00	05-09-2013	4.85	9.82
FMK_45_T1	Broadleaf	455169.00	6292837.00	05-09-2013	5.33	9.34
FMK_45_T2	Broadleaf	455134.00	6292894.00	05-09-2013	4.70	8.17

CCRS28	Conifer	451270.15	6311992.77	21-07-2012	4.85	8.68
CCRS28B	Conifer	451270.15	6311992.77	21-07-2012	4.67	8.42
CCRS103	Conifer	475803.92	6347568.73	22-07-2012	3.00	4.94
MATC1	Conifer	465603.49	6316619.72	22-07-2012	3.64	8.33
MATC3	Conifer	465524.81	6316645.75	22-07-2012	4.11	7.87
MATC4	Conifer	465463.60	6316687.59	22-07-2012	3.51	6.57
CCRS131	Conifer	474584.73	6346149.61	23-07-2012	3.34	6.88
CCRS133	Conifer	474563.47	6346125.70	23-07-2012	3.99	6.92
CCRS134	Conifer	474534.88	6345150.47	23-07-2012	1.86	3.26
CCRS135	Conifer	474508.90	6345196.16	23-07-2012	4.21	6.84
CCRS136	Conifer	474510.95	6345078.61	23-07-2012	3.37	5.34
CCRS143	Conifer	474535.53	6344008.77	23-07-2012	2.95	5.37
CCRS154	Conifer	461093.03	6348892.43	23-07-2012	4.20	7.88
CCRS154B	Conifer	461093.03	6348892.43	23-07-2012	3.70	7.88
CCRS159	Conifer	465764.64	6317012.79	23-07-2012	2.40	3.58
CCRS161	Conifer	465764.72	6316807.69	23-07-2012	3.95	6.99
MATC12	Conifer	465785.98	6316763.32	23-07-2012	3.02	4.84
MATC12B	Conifer	465785.98	6316763.32	23-07-2012	2.26	4.84
MATC4B	Conifer	465463.60	6316687.59	23-07-2012	3.12	6.30
MATC5	Conifer	465655.21	6316986.00	23-07-2012	4.75	7.54
MATC5B	Conifer	465655.21	6316986.00	23-07-2012	4.35	7.54
MATC6	Conifer	465639.08	6317166.18	23-07-2012	3.48	6.17
MATC6B	Conifer	465639.08	6317166.18	23-07-2012	3.70	6.69
MATC7	Conifer	465697.00	6316951.33	23-07-2012	3.85	7.07
MATC7B	Conifer	465697.00	6316951.33	23-07-2012	3.50	7.05
MATC8	Conifer	465803.64	6317126.03	23-07-2012	3.39	6.67
MATC8B	Conifer	465803.64	6317126.03	23-07-2012	3.13	6.65
CCRS205	Conifer	450905.42	6294255.04	24-07-2012	4.77	8.40
CCRS207	Conifer	450923.92	6294364.51	24-07-2012	3.83	5.97

CCRS246	Conifer	466965.97	6316484.32	25-07-2012	4.57	8.85
CCRS261	Conifer	459450.63	6346936.33	25-07-2012	3.77	5.94
CCRS270	Conifer	465384.94	6338891.34	25-07-2012	3.83	5.90
CCRS11	Conifer	452372.00	6294449.00	30-07-2012	5.34	11.11
CCRS13 Navus	Conifer	452355.00	6294402.00	30-07-2012	4.96	11.30
CCRS2 Navus	Conifer	454700.00	6293625.00	30-07-2012	4.53	7.79
CCRS205 Navus	Conifer	465373.00	6317311.00	30-07-2012	4.60	7.80
CCRS206 Navus	Conifer	465309.00	6317248.00	30-07-2012	3.25	6.10
CCRS207 Navus	Conifer	464918.00	6317490.00	30-07-2012	4.60	6.51
CCRS3 Navus	Conifer	454801.00	6293638.00	30-07-2012	4.41	6.29
CCRS3 Navus2	Conifer	454801.00	6293638.00	30-07-2012	5.01	8.42
CCRS8 Navus	Conifer	453890.00	6294220.00	30-07-2012	5.45	10.78
CCRS8 Navus2	Conifer	453871.00	6294215.00	30-07-2012	4.85	7.80
CCRS9 Navus	Conifer	453736.00	6294234.00	30-07-2012	4.33	8.00
CCRS9 Navus2	Conifer	453755.00	6294233.00	30-07-2012	4.00	7.80
FMK_10_T1	Conifer	451089.00	6311621.00	04-09-2013	4.74	9.56
FMK_10_T2	Conifer	451092.00	6311592.00	04-09-2013	4.89	9.95
FMK_11_T1	Conifer	451070.00	6311540.00	04-09-2013	4.15	9.51
FMK_11_T2	Conifer	451073.00	6311510.00	04-09-2013	3.82	9.80
FMK_12_T1	Conifer	451169.00	6311642.00	04-09-2013	4.33	10.42
FMK_12_T2	Conifer	451173.00	6311672.00	04-09-2013	4.17	9.39
FMK_13_T1	Conifer	451168.00	6311562.00	04-09-2013	4.12	10.40
FMK_13_T2	Conifer	451168.00	6311590.00	04-09-2013	4.17	9.39
FMK_18_T1	Conifer	451648.00	6311953.00	04-09-2013	4.49	8.59
FMK_18_T2	Conifer	451680.00	6311942.00	04-09-2013	4.06	7.83
FMK_36_T1	Conifer	451537.00	6312017.00	04-09-2013	3.85	7.02
FMK_36_T2	Conifer	451568.00	6312005.00	04-09-2013	4.02	6.41
FMK_37_T1	Conifer	458732.00	6311406.00	04-09-2013	3.01	5.67
FMK_37_T2	Conifer	458760.00	6311401.00	04-09-2013	2.88	5.41

FMK_38_T1	Conifer	458651.00	6311291.00	04-09-2013	4.46	7.77
FMK_38_T2	Conifer	458675.00	6311279.00	04-09-2013	3.87	8.09
FMK_39_T1	Conifer	458017.00	6311514.00	04-09-2013	3.57	5.52
FMK_39_T2	Conifer	457989.00	6311528.00	04-09-2013	3.30	6.48
FMK_40_T1	Conifer	457738.00	6311523.00	04-09-2013	3.25	5.80
FMK_40_T2	Conifer	457708.00	6311521.00	04-09-2013	2.88	6.41
FMK_41_T1	Conifer	457903.00	6311522.00	04-09-2013	3.02	5.41
FMK_41_T2	Conifer	457871.00	6311522.00	04-09-2013	2.40	5.27
FMK_9_T1	Conifer	451363.00	6311631.00	04-09-2013	3.90	6.98
FMK_9_T2	Conifer	451345.00	6311660.00	04-09-2013	3.50	7.41
FMK_26_T1	Conifer	456310.00	6291298.00	05-09-2013	3.75	7.61
FMK_26_T2	Conifer	456282.00	6291324.00	05-09-2013	3.84	8.02
FMK_42_T1	Conifer	455273.00	6292507.00	05-09-2013	4.81	10.53
CCRS33B	Disturbed	450528.86	6312915.98	21-07-2012	2.31	4.41
CCRS132	Disturbed	474593.64	6346088.94	23-07-2012	1.86	3.11
FMK_15_T1	Disturbed	465379.00	6311418.00	04-09-2013	3.76	6.56
FMK_15_T2	Disturbed	465388.00	6311390.00	04-09-2013	4.24	6.58
FMK_16_T1	Disturbed	465495.00	6311444.00	04-09-2013	2.64	6.15
FMK_16_T2	Disturbed	465467.00	6311439.00	04-09-2013	2.94	6.50
FMK_33_T2	Disturbed	470072.00	6330674.00	05-09-2013	0.20	0.61
FMK_35_T1	Disturbed	470068.00	6330751.00	05-09-2013	0.60	0.90
FMK_33_T1	Disturbed	470040.00	6330670.00	05-09-2013	0.09	0.64
FMK_35_T2	Disturbed	470037.00	6330763.00	05-09-2013	0.70	1.10
CCRS101	Grass/Exp	475806.74	6347500.80	21-07-2012	0.52	0.70
CCRS30	Grass/Exp	451133.46	6312227.14	21-07-2012	1.65	2.08
CCRS30B	Grass/Exp	451133.46	6312227.14	21-07-2012	0.68	2.08
CCRS102	Grass/Exp	475806.74	6347500.80	22-07-2012	1.65	2.24
CCRS102B	Grass/Exp	475806.74	6347500.80	22-07-2012	1.36	2.24
CCRS106	Grass/Exp	474982.71	6347405.83	22-07-2012	2.87	4.71

CCRS106B	Grass/Exp	474982.71	6347405.83	22-07-2012	2.30	4.71
CCRS110	Grass/Exp	474978.01	6347606.71	22-07-2012	0.97	1.30
CCRS110B	Grass/Exp	474978.01	6347606.71	22-07-2012	0.82	1.00
CCRS120	Grass/Exp	474373.04	6346628.46	22-07-2012	2.01	3.69
CCRS130	Grass/Exp	474599.19	6346108.86	23-07-2012	1.81	3.11
CCRS137	Grass/Exp	474497.76	6345005.87	23-07-2012	0.26	0.60
CCRS141	Grass/Exp	474649.71	6344049.32	23-07-2012	2.90	5.11
CCRS142	Grass/Exp	474541.17	6344020.38	23-07-2012	2.11	3.09
CCRS142B	Grass/Exp	474541.17	6344020.38	23-07-2012	1.23	3.09
CCRS145	Grass/Exp	474854.23	6343684.35	23-07-2012	0.62	0.98
CCRS148	Grass/Exp	474826.74	6343558.56	23-07-2012	0.63	1.47
CCRS148B	Grass/Exp	474826.74	6343558.56	23-07-2012	0.42	1.47
CCRS157	Grass/Exp	465758.28	6317102.74	23-07-2012	2.36	3.56
CCRS163	Grass/Exp	465837.12	6316540.24	23-07-2012	0.88	2.70
CCRS203	Grass/Exp	450831.37	6294323.76	24-07-2012	0.30	0.78
CCRS208	Grass/Exp	450888.71	6294368.83	24-07-2012	0.39	0.82
CCRS255	Grass/Exp	460251.31	6343288.66	25-07-2012	1.29	2.13
CCRS257	Grass/Exp	460222.25	6343280.15	25-07-2012	2.68	4.97
CCRS259	Grass/Exp	460048.77	6344726.52	25-07-2012	1.72	4.44
CCRS274	Grass/Exp	460315.87	6343285.74	25-07-2012	0.57	1.68
CCRS278	Grass/Exp	459392.48	6346937.30	25-07-2012	1.46	2.91
CCRS202 Navus	Grass/Exp	454507.00	6293898.00	30-07-2012	1.60	2.94
CCRS27	Wetland	451244.96	6312178.26	21-07-2012	3.48	7.11
CCRS27B	Wetland	451244.96	6312178.26	21-07-2012	4.08	7.11
CCRS34	Wetland	450446.82	6312947.86	21-07-2012	4.41	6.43
CCRS34B	Wetland	450446.82	6312947.86	21-07-2012	3.61	6.43
CCRS35	Wetland	450237.03	6312937.99	21-07-2012	4.69	10.12
CCRS105	Wetland	475721.09	6347518.21	22-07-2012	3.57	5.95
CCRS105B	Wetland	475721.09	6347518.21	22-07-2012	4.04	5.95

CCRS107	Wetland	474904.91	6347493.25	22-07-2012	2.74	4.27
CCRS107B	Wetland	474904.91	6347493.25	22-07-2012	2.70	4.27
CCRS112	Wetland	474990.15	6347665.38	22-07-2012	2.06	3.96
CCRS112B	Wetland	474990.15	6347665.38	22-07-2012	2.23	3.96
CCRS114	Wetland	474567.52	6346635.17	22-07-2012	4.07	6.91
CCRS116	Wetland	474453.80	6346622.30	22-07-2012	2.95	5.14
CCRS140	Wetland	474684.76	6344094.08	23-07-2012	4.26	7.57
CCRS209	Wetland	452282.95	6294476.01	24-07-2012	4.46	8.74
CCRS272	Wetland	460356.46	6343293.56	25-07-2012	2.12	4.46
CCRS11B	Wetland	452364.00	6294450.00	30-07-2012	4.53	11.11
CCRS12 Navus	Wetland	452239.00	6294514.00	30-07-2012	1.76	4.48
CCRS25 Navus	Wetland	454907.00	6311054.00	30-07-2012	4.30	7.76
CCRS29 Navus	Wetland	450986.00	6312115.00	30-07-2012	3.76	6.90
CCRS31 Navus	Wetland	451058.00	6312432.00	30-07-2012	1.39	1.71
CCRS33 Navus	Wetland	450570.00	6312877.00	30-07-2012	3.26	4.99
CCRS34 Navus	Wetland	450502.00	6312886.00	30-07-2012	3.59	6.64
CCRS6 Navus	Wetland	454365.00	6293912.00	30-07-2012	2.76	5.57
FMK_34_T1	Wetland	467703.00	6331926.00	05-09-2013	4.36	6.18
FMK_34_T2	Wetland	467726.00	6331899.00	05-09-2013	3.51	6.56
CCRS140B	Wetland	474684.76	6344094.08	23-07-2012	4.49	7.57